MDPI

Article

Carbonaceous Materials in the Longmenshan Fault Belt Zone: 3. Records of Seismic Slip from the Trench and Implications for Faulting Mechanisms

Jialiang Si [1],* [ID], Haibing Li [1], Li-Wei Kuo [2] [ID], Jyh-Rou Huang [3], Sheng-Rong Song [4], Junling Pei [5], Huan Wang [1], Lei Song [6], Jiann-Neng Fang [7] and Hwo-Shuenn Sheu [8]

[1]   Key Laboratory of Deep-Earth Dynamics of Ministry of Natural Resources, Institute of Geology, Chinese Academy of Geological Sciences, Beijing 100037, China; lihaibing06@163.com (H.L.); wanghuan4585@126.com (H.W.)

[2]   Department of Earth Sciences, National Central University, Taoyuan 320, Taiwan; liweikuo@ncu.edu.tw

[3]   Department of Earth Sciences, National Taiwan Normal University, Taipei 106, Taiwan; hjrou0906@hotmail.com

[4]   Department of Geosciences, National Taiwan University, Taipei 106, Taiwan; srsong@ntu.edu.tw

[5]   Institute of Geomechanics, Chinese Academy of Geological Sciences, Beijing 100081, China; peijl@aliyun.com

[6]   Boyue Instruments (Shanghai) Co., Ltd., Shanghai 201612, China; m.song@boyuesh.com

[7]   National Taiwan Museum, Taipei 100, Taiwan; jnfang@ntm.gov.tw

[8]   National Synchrotron Radiation Research Center, Hsinchu 30076, Taiwan; hsheu@nsrrc.org.tw

*   Correspondence: gongrenbaqin@126.com; Tel.: +86-10-6899-0664

check for updates

Abstract: In recent studies on the recognition of graphitized gouges within the principal slip zone (PSZ) of the Longmenshan fault in China, we proposed that the presence of graphite might be evidence of fault slip. Here, we characterized the clay- and carbonaceous-rich gouges of the active fault zone of the Longmenshan fault belt using samples collected from the trench at Jiulong, which was deformed during the 2008 M_W-7.9 Wenchuan earthquake, to determine if graphite is present and study both the processes influencing fault behavior and the associated faulting mechanism. Mineralogical and geochemical analyses of the Jiulong trench sample show the presence of a hydrothermal mineral (i.e., dickite) integrated with dramatic relative chemical enrichment and relative depletion within a yellowish zone, suggesting the presence of vigorous high-temperature fluid–rock interactions, which are likely the fingerprint of thermal pressurization. This is further supported by the absence of carbonaceous materials (CMs) given the spectrometric data obtained. Interestingly, the Raman parameters measured near the carbonaceous-rich gouge fall within the recognized range of graphitization in the mature fault zone, implying the origin of a mature fault, as shown in the companion paper. According to both the sharp boundary within the very recent coseismic rupture zone of the 2008 M_W-7.9 Wenchuan earthquake and the presence of kinetically unstable dickite, it is strongly implied that the yellow/altered gouge likely formed from a recent coseismic event as aconsequence of hydrothermal fluid penetration. We further surmise that the CM characteristics varied according to several driving reactions, e.g., transient hydrothermal heating versus long-term geological metamorphism and sedimentation.

Keywords: carbonaceous materials; trench; Longmenshan fault zone; faulting mechanism

1. Introduction

There is a close relationship between fault rock properties and the slip of major faults. For example, faults and related fractures play important roles in fluid migration throughout the upper crust [1,2],

while fluid circulation in faults can affect fault mechanical behavior by influencing the distributions of temperature and pressure and the composition of fault-related rocks, which in turn influence the dominant deformation mechanisms and fault rheology. In particular, it has been recognized in various major fault zones that elevated pore fluid pressure could reduce effective confining stress and induce frictional slip under low fault stress [3–6]. Fault zones can be considered fluid-flow conduit/barrier systems that vary over time and space during the lifetime of a fault. Additionally, fluids have been suggested to have either passive or active effects during the seismic cycle [7]. At shallow to moderate depths in the crust (<10 km), there are many potential fluid sources, including meteoric, metamorphically derived, connate, basin and hydrothermal fluids [8–14]. Fluids can alter mineral assemblages and the rates of chemical and mechanical processes during and after deformation, potentially leading to the weakening of fault-related rocks and the localization of slip in fault zones, thus affecting various faulting mechanisms, such as reaction weakening, thermal pressurization hydrolytic weakening and even healing [4,5,8,15–18].

The Longmenshan fault belt is at the transition zone between the eastern margin of the Tibetan Plateau and Sichuan basin, and it is mainly composed of three north-east (NE)-striking thrust faults: (from west to east) the Wenchuan-Maoxian, Yingxiu-Beichuan, and Guanxian-Anxian faults. The 12 May 2008 Wenchuan earthquake (M_W 7.9) occurred along the Longmenshan fault belt, and two coseismic surface ruptures of approximately 270 and 80 km developed along the Yingxiu–Beichuan and Guanxian-Anxian faults, respectively, and were characterized by simple thrust faulting coupled with dextral slip and pure thrusting features, respectively [19–23]. Determining why such a large difference occurred between the two rupture faults in one earthquake was a major goal of the Wenchuan Earthquake Fault Scientific Drilling Project (WFSD), which started less than 200 days after the earthquake. The Anxian-Guanxian fault at the front of the Longmenshan fault zone, located 10-15 km east of the Yingxiu-Beichuan fault, ruptured north-eastward from the Zipingpu reservoir, mainly along the pre-existing thrust fault between the Triassic sandstone and the Jurassic sandstone conglomerate. The rupture zone is mainly composed of folding structures. The rupture fault plane has a significantly lower dip angle than the Yingxiu–Beichuan rupture, and it is characterized by an almost pure thrust motion with a vertical displacement of 2–3 m and a maximum displacement of approximately 4 m. The well-exposed outcrop in Jiulong town represents an especially ideal case to study the fluid flow mechanisms and fluid–rock interactions that occur during faulting.

Coseismic graphitization, which was first revealed from both the gouge samples and the experimental samples collected during WFSD-1 drilling on the Yingxiu-Beichuan fault, was likely driven by the frictional heating of carbonaceous materials (CM) due to strain rather than strain rate and might be a potential seismic indicator for the fault investigation of the extremely stable features of graphite [24,25].

This paper presents the results of an integrated fieldgeochemical and mineralogical study on the deformation of the Anxian-Guanxian fault, the frontal Longmenshan fault zone, and the south-eastern margin of the Tibetan plateau in China. A trench cutting across the coseismic rupture zone that developed during the 2008 Wenchuan earthquake (M_W 7.9) allows us to characterize the fault structures from the microscale to the trench-scale. We use X-ray fluorescence (XRF), X-ray diffraction (XRD) and Raman spectroscopy to reveal fluid-rock interactions and examine how CM may have varied in several segments of the fault zone. Finally, we integrate these results and discuss the characteristics of graphitization by comparing the results with the results obtained from deep drilling samples.

2. Materials and Methods

According to the surface outcrop, there are obvious differences in the color and lithology of the hanging wall and footwall of the Anxian-Guanxian fault (Figure 1), where the fault plane distinctively lies between the upward black Triassic strata and the downward reddish-brown to grayish-green Jurassic strata. Field investigation shows that the Anxian–Guanxian surface rupture zone strikes N10° E and dips to the west, crossing the river and producing a maximum vertical offset of 4.2 m in the

Qingquan village of the Jiulong County of Mianzhu City [21]. A 10 m-long, 3 m-deep, and 2.5 m-wide trench was excavated across the rupture zone at that location (Figure 1) [26]. The Wenchuan earthquake slip zone, which is clearly visible in the trench profile, is sharp and dips to the northwest with a dip angle of 60°. On the west side, i.e., the hanging wall, there are an approximately 1.0 m-thick dark-colored foliated fault gouge and an approximately 0.5 m-thick gray fault gouge, as well as some fault breccia with oriented structures. On the east side of the slip plane, i.e., the footwall, there is grayish-green and reddish-brown Jurassic sandstone with little or no fractures. There is a clear asymmetrical fault zone structure, i.e., fault gouges, fault breccia, and/or fractures, developed in the hanging wall. This structure is similar to that of the Nojima fault zone in Japan [27].
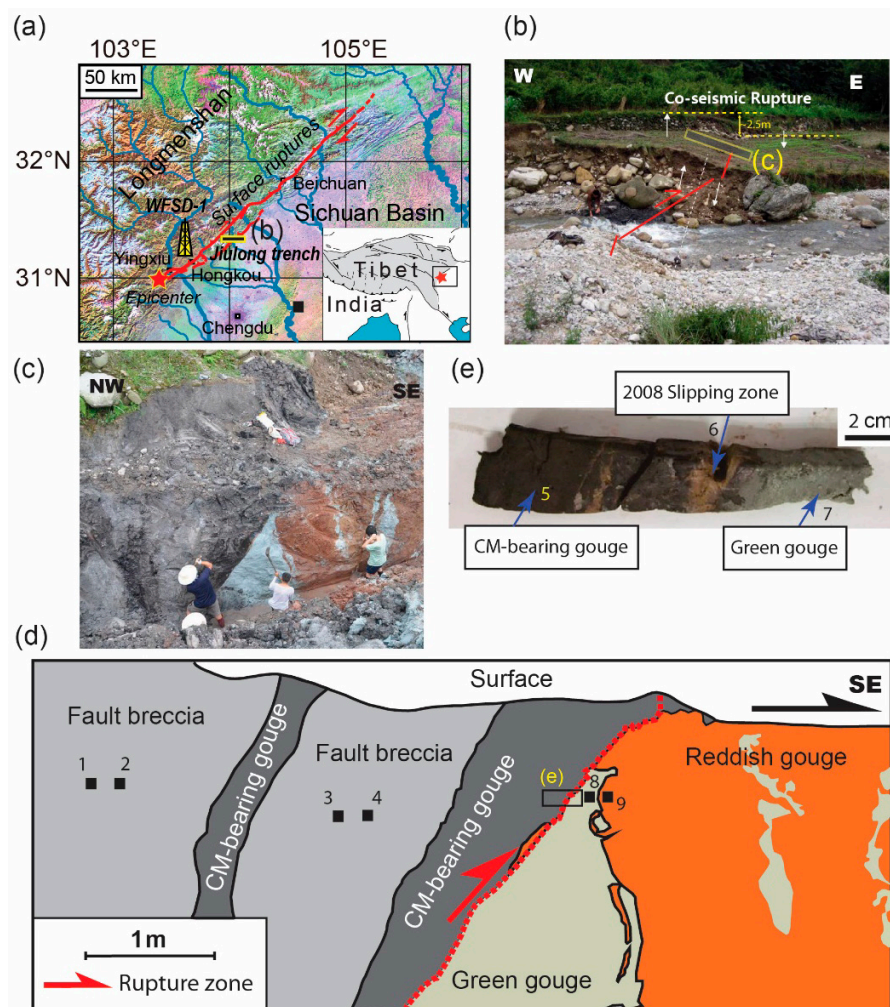

Figure 1. Map and images showing the front Longmenshan fault zone, the coseismic surface rupture zone formed in the 2008 M_W-7.9 Wenchuan earthquake in China, the trench of the Anxian-Guanxian fault, and a collected fault sample. (**a**) The two surface rupture zones associated with the M_W-7.9 earthquake and the location of the Wenchuan Earthquake Fault Scientific Drilling Project (WFSD-1) site. The red star is the epicenter of the main shock. The inset is a schematic of the Tibetan Plateau. The yellow area shows the location of (**b**). (**b**) The Anxian-Guanxian surface rupture outcropped at the town of Jiulong. The largest vertical displacement along the Anxian-Guanxian fault surface rupture was approximately 4 m and located in the Qingquan village; the vertical offset was approximately 2.5 m at the trench site during the Wenchuan earthquake. The yellow rectangle shows the trench construction site of (**c**). (**c**) Image of the trench. (**d**) Sketch of the trench; the numbers label the samples, and the black box shows the sampling location of sample numbers 5, 6 and 7. (**e**). An image of a sample.

In this study, the classification of the fault-related rocks follows the textural classification of [28]. A fault zone can be divided into three components: the fault core, the damage zone and the undeformed protolith; the fault core accommodates slip and is often accompanied by a low-permeability gouge or mineral precipitates [4,29].

In the trench, the fault gouge is mainly gray, dark gray and black (Figure 1). CM can be observed in some fault gouges. The detailed statistics of the cores show that the CM layers are mostly distributed in or near the fault breccia and fault gouge, suggesting that CM might be related to fault activity [30].

Focusing on the principal slip zone (PSZ) of the 2008 Wenchuan earthquake, we collected a fresh 75-mm-long sample from the trench and used a M4 TORNADO (Bruker, Berlin, Germany) for micro-XRF analysis (Figure 2).
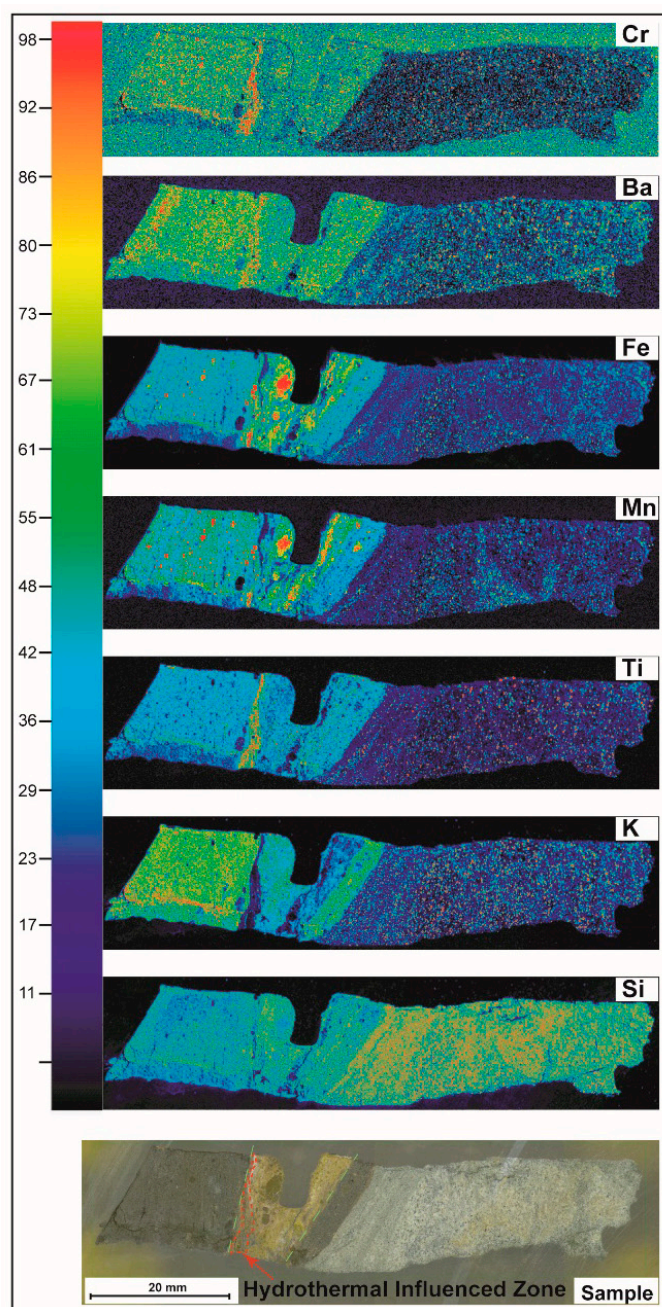

Figure 2. X-ray fluorescence (XRF) map of the Jiulong trench samples. The 2008 slip zone lies at the top of the middle yellowish gouge layer. The chromatographic column numbers indicate the element abundances. The red lines show the location of the hydrothermal influenced zone (HIZ).

We also collected 10 samples (from west to east) across the PSZ, covering the fault breccia and fault gouge of various colors. All samples were crushed into powder with an agate mortar and pestle, mixed with distilled water and coated on glass slides. We used a PANalytical X'Pert PRO X-ray diffractometer at the National Taiwan University under the following conditions: filtered CuKα (1.540 Å) radiation, a 45-kV 40-mA X-ray generator, a 1.0°/min scanning speed, and a 5°–40° 2θ coverage (Figure 3) (please see [31] for details).
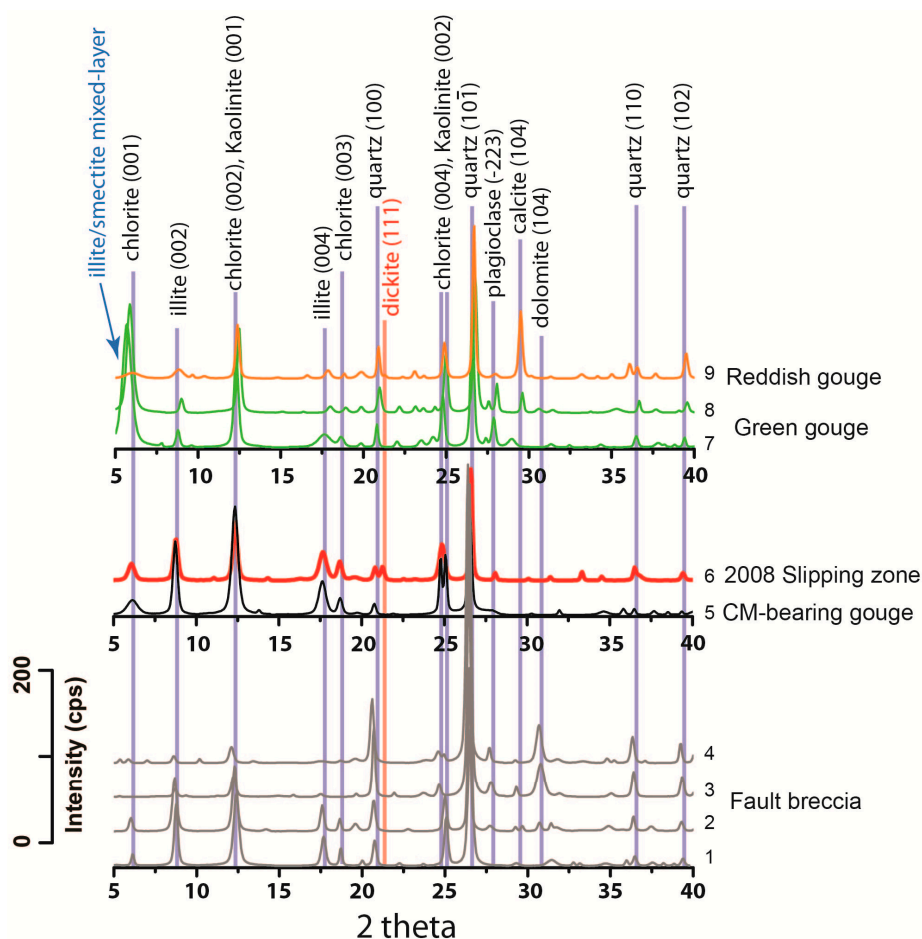

Figure 3. Characterization of the mineral phases of the Jiulong trench samples. The mineral phases of the breccia are very similar to those of the gouge zone. The X-ray diffraction (XRD) data of the carbonaceous material (CM)-bearing gouge demonstrate the presence of dickite (cps: counts per second).

Raman spectroscopy can be an ideal tool for CM analysis [32]. Using the Horiba Jobin Yvon ultraviolet-visible (UV-VIS) Labram HR Micro-Raman spectrometer at the National Taiwan Museum, Taipei, Taiwan, we obtained Raman spectra of the CM (RSCM) on the sample glass slides at room humidity with an excitation beam wavelength of 532 nm and a laser power of 5 mW without neutral density filters; during this process, we focused on the 1100–1800-cm^{-1} region of the Raman spectrum, which includes all first-order bands of CM (as suggested by [33]). The first-order bands include the graphite band (from 1575 cm^{-1} to 1592 cm^{-1}), which is known as the G band, and two disorder-induced bands, referred to as the "D1 band" (from 1330 cm^{-1} to 1336 cm^{-1}) and the "D3 band" (from 1490 cm^{-1} to 1525 cm^{-1}) (Figure 4 inset). The relevant parameters of the Raman spectrum (i.e., peak height, peak width, and peak position) were evaluated by fitting the pseudo-Voigt function (Gaussian-Lorentzian linear combination) [34,35]. In addition, two indicative parameters introduced by [25] were employed: (1) the D1/G width ratio versus peak height ratio (Figure 5a) and (2) the D1 and G widths normalized over the average for all samples versus their peak positions (Figure 5b).
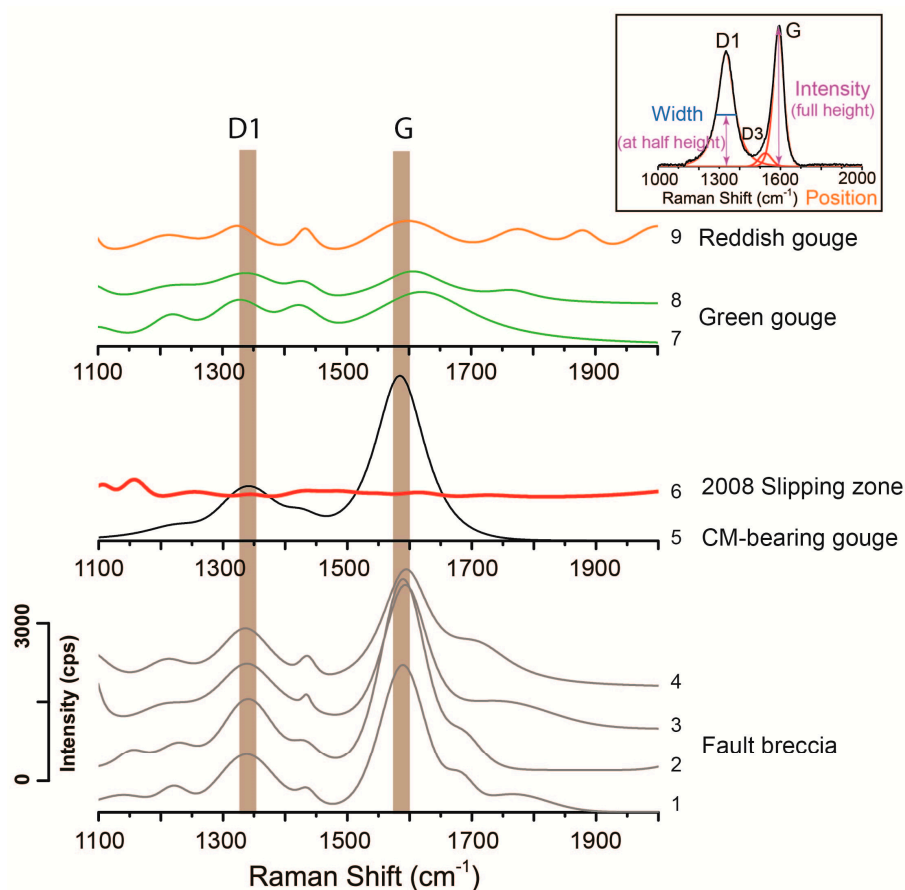
Figure 4. The representative first-order region of the Raman spectra for several fault components in the trench. The inset shows the criteria for defining the indicative parameters derived from the relevant spectrum decomposition (width, intensity, peak position, etc.).

3. Results

3.1. X-Ray Fluorescence (XRF) Analysis

A XRF mapping of several typical elements are plotted for the 75 mm-long segment (Figure 2). According to the data, most elements (Cr, Ba, Fe, Mn, Ti, K) are significantly relatively enriched in the hanging wall, and only silicon is remarkably relatively enriched in the foot wall. In the hydrothermal influenced zone (HIZ), some elements (Fe, Mn, Si) are relatively enriched, while others (Cr, Ba and K) are relatively depleted. However, if we check the data carefully, at the top of the PSZ, the possible slip plane of the 2008 Wenchuan earthquake, three elements (Cr, Ba, Ti) are obviously relatively enriched. Potassium is clearly relatively depleted. Another notable feature is the inverse relationship between titanium and the other two elements (iron and magnesium).

3.2. X-Ray Diffraction (XRD) Analysis

The XRD patterns derived from the various fault components of the trench (breccia and gouge) are separately plotted (Figure 3). Fault components are labeled by color in the XRD patterns (e.g., the fault breccia samples are shown in gray). The common way to distinguish kaolinite from chlorite is heating to 550 °C, which generally destroys the structure of chlorite after determination, thus a different option to determine the presence of kaolinite and chlorite is used here, i.e., the peak position at 2θ of approximately 25° (3.57/3.54 Å) [36]. The common mineral assemblages from the fault breccia to the reddish gouge are identified as chlorite, illite, kaolinite and quartz. In particular, the XRD patterns of the PSZ of the 2008 Wenchuan earthquake show the presence of an unusual mineral that is absent in

the surrounding zones. The intensity at 2θ of approximately 27.6° is smaller than the one at 2 theta of approximately 21.2°, which strongly suggests that the peak does not consist of feldspar but can mainly be attributed to the kaolinite group. Moreover, the unusual peaks that only appeared in the chemical anomaly zone are likely derived from hot fluid alteration. Thus, dickite is the most likely option. Notably, within the fault core of the surface rupture zone, i.e., the CM-bearing gouge and the PSZ, there are numerous tiny peaks that indicate the complexity of the mineral phases. Similar to what has been reported [31,37,38], the occurrence and formation of chlorite and illite/smectite mixed-layer minerals might imply certain information about faulting or weathering, which will be revealed by systematic microstructural examination and mineralogical examination in the near future.

3.3. Raman Spectroscopy

The RSCM of the various fault components of the Jiulong trench (breccia and gouge) are plotted separately (Figure 4). All Raman spectra are differentiated by color for all fault components, including the fault breccia, the CM-bearing gouge, the 2008 PSZ, the green gouge and the reddish gouge. Five measurements per sample were conducted on several sample spots, and each spot was measured with three integration times of 5 s each. The spectral parameters (G and D1) of each sample were determined as the average values from 10 Raman analyses. The Raman analysis spectrum was calibrated with a Si-waver before each set of measurement. The curve fitting in our study is likely influenced by individual operators and might be processed with a standardized curving-fitting procedure in the future, as suggested by Lünsdorf [39,40]. According to the representative first-order region of the Raman spectra, the D1 band and G band of the trench samples are at approximately 1335 cm^{-1} and 1580 cm^{-1}, respectively. Notably, there is no evidence of CM along the 2008 slip zone. In addition, the hanging wall samples (i.e., the fault breccia and the CM-bearing gouge) contain a more intense difference than the footwall samples (i.e., the green gouge and the reddish gouge) between the G band and the D1 band. There is a shift in the G band of the gouge samples towards a higher frequency than that of the breccia samples.

The CM-bearing gouge sample has a distinctively low D1/G intensity ratio and D1/G width ratio when compared to the breccia samples (Figure 5a). In addition, most of the gouge samples contain a higher frequency D1 band position (~1340 cm^{-1}) than the breccia samples (~1330 cm^{-1}), and the G band of the CM-bearing gouge has a higher frequency and a smaller peak width ratio (Figure 5b). The CM-bearing gouge sample has similar Raman parameter characteristics; that is, compared to the breccia samples, the gouge sample has a high R1 value and low G band peak width ratio. Figure 5 reports the FZ590 Raman data [24] integrated for the discussion of fault maturity.
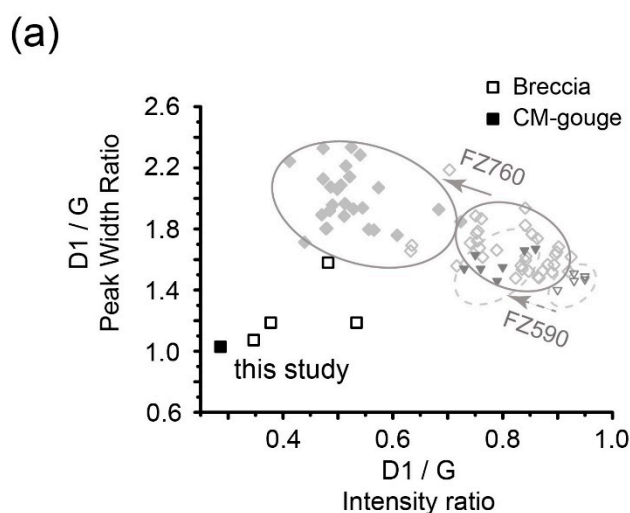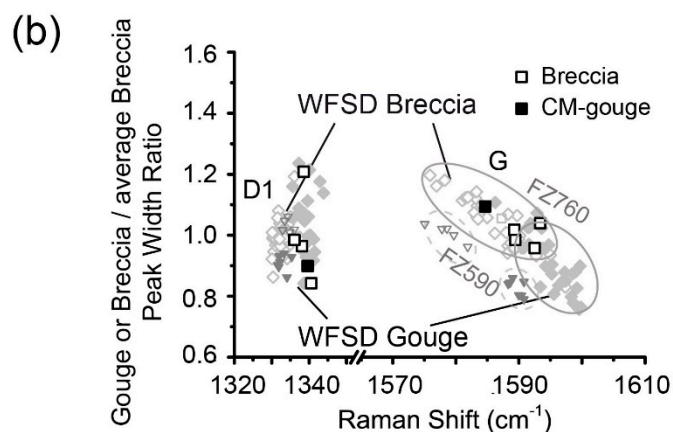

Figure 5. *Cont.*

Figure 5. Decomposition of the Raman spectra of the Jiulong trench samples. (**a**) D1/G peak width ratio versus D1/G intensity ratio. The FZ590 and FZ760 results of the WFSD-1 are also included [24,41]. (**b**) G peak width of the CM-bearing gouge over the average breccia peak width versus the G band peak position. The FZ590 and FZ760 results of the WFSD-1 are also included [24,41].

4. Discussion and Conclusions

The XRF data of the Jiulong samples studied show two chemical characteristic domains: the hanging wall CM-bearing gouge is characterized by relatively high contents of Al, Fe, K, Mn, Ba, and Ti, whereas the foot wall green gouge is mainly composed of a relatively high content of Si (Figure 2). The chemical characteristics of the trench samples might be derived from the various host lithologies [30]. However, the fractures and fissures were mainly observed in the hanging wall of the Jiulong trench. Surface weathering was likely more efficient in the hanging wall than in the footwall and should be considered for the characterization of chemical properties of the outcrop.

The hanging wall CM-bearing gouge is sandwiched by a yellowish gouge (Figures 1 and 2). The chemical composition of the yellowish gouge, which is characterized by relatively high contents of Al, Fe, K, Mn, Ba, and Ti, is more similar to that of the hanging wall CM-bearing gouge than to that of the foot wall green gouge. In addition, the mineral phases of the yellowish gouge are identical those of the hanging wall CM-bearing gouge (Figure 3). Taken together, these results suggest that the source rock of the yellowish gouge was derived from the CM-bearing gouge. Interestingly, a chemical anomaly, including a relative enrichment of Ti and relative depletion of K, was observed in a small localized patch within the yellowish gouge (~1 mm thick). The elements Ti and K are widely accepted as indices for evaluating the elemental variations in brittle fault zones because of their differential mobilities during fluid–rock interactions [18,42–44]. In addition, integrated with the presence of dickite, a hydrothermal mineral [43–47], the chemical anomaly zone indicates the possibility of high-temperature fluid–rock interactions.

CM graphitization is widely used as a temperature indicator for long-term geological metamorphism and sedimentation [48,49], but its applicability for estimating the achieved maximum temperature during seismic fault slip remains uncertain [35]. Because the effects of increasing temperature on the structural diversity of CM remains unclear, the determination of the associated CM characteristics and their relevant applications to fault deformation are challenging. Regarding the Longmenshan fault in China, current studies have shown divergent CM graphitization. Kouketsu et al. (2017) [50] collected samples from the surface outcrop of the southern Longmenshan fault and characterized naturally and experimentally deformed products. They found no evidence of CM graphitization and suggested that the graphite was probably either formed locally or not formed during seismic fault motion. However, Kuo et al. (2014) [24] collected samples for the Wenchuan Earthquake Fault Scientific Drilling Project-1 (WFSD-1) from the southern Longmenshan fault and analyzed naturally and experimentally deformed products; they suggested that CM graphitization likely occurred within the active fault zone of the Longmenshan fault during the 2008 M_W-7.9

Wenchuan earthquake. In addition, Kuo et al. (2017) [25] demonstrated that CM graphitization is induced by high-temperature pulses attributed to seismic fault slips. The geological records of the active fault zone of the Longmenshan fault seemingly show divergent CM graphitization, likely due to both the varied CM structures and the friction work experienced during earthquakes from depth to surface outcrop.

Our data show an absence of CM within the HIZ (Figure 4) and conflict with the reported occurrence of CM in the Longmenshan fault [24,25,50]. The yellowish HIZ at Jiulong shows the presence of dickite (Figure 3) integrated with a relative enrichment of Ti and a relative depletion of K (Figure 2), which might indicate the injection of high-temperature fluid-rock interaction products. Interestingly, a similar occurrence (i.e., the absence of CM within the PSZ) was reported in the active Chelungpu fault in Taiwan. The Chelungpu thrust fault ruptured northward approximately 90 km as a result of the M_W-7.6 Chi-Chi earthquake, which struck central Taiwan on 21 September 1999 [51,52]. After the 1999 Chi-Chi earthquake, the Taiwan Chelungpu Fault Drilling Project (TCDP) was initiated to address the urgent need to fill knowledge gaps, e.g., how fault material properties drive catastrophic slide rather than creep. Current analyses of TCDP materials, including mineralogical, geochemical, magnetic, and microstructural evidence, show that the active fault zone of the Chelungpu fault experienced high-temperature fluid (thermal) pressurization, presumably driven by coseismic faulting [36,51,53,54]. Importantly, Hirono et al. (2015) analyzed TCDP samples with products from heating and frictional experiments [55]. They suggested that the absence of CM in the Raman spectra, as well as in the infrared (IR) spectra, resulted from thermal decomposition and condensation reactions during pyrolysis, which was likely driven by thermal pressurization. Thus, pyrolysis may play a role in the present case, but further analyses are required to fully understand the pyrolysis of CM.

The determination of the origin of the yellow/altered gouge remains challenging. Two lines of evidence strongly imply the yellow/altered gouge likely formed from a recent coseismic event: (1) the yellow/altered gouge was found at a sharp boundary within the very recent coseismic rupture zone (from the M_W-7.9 Wenchuan earthquake); and (2) the presence of dickite, which is kinetically unstable on the surface, was likely formed recently instead of over a long geological time period. Therefore, it is strongly implied that the formation of the yellow/altered gouge is relevant to the coseismic event. Because thermal pressurization is a widespread and prominent process for fault weakening [56], it was postulated to have occured in the 2008 Wenchuan earthquake [57], although the effective normal stresses near the surface are too low to meet the requirement of thermal pressurization. Thus, in this study, we suggest that the yellow/altered gouge is a consequence of hydrothermal fluid penetration, rather than of a deeper place where thermal pressurization occurred. The driving force and released energy (frictional heat) of thermal pressurization decline at the end of fault propagation, and the remaining high-temperature fluid should cool and migrate to produce the chemical element variations. Additionally, the shape of HIZ suggests upward injection. As the 2D micro-XRF mapping only visualized the distribution of the elements and was not quantitative, the method underlying the currently reported volume loss during fluid–rock interactions will require future study.

In addition, we compared the RSCM data with those from the fault zones of the WFSD-1 (located at depths of 590 m and 760 m, which were named FZ590 and FZ760, respectively). In general, the CM-bearing gouge from the Jiulong trench shows RSCM characteristics similar to those of FZ760 (Figure 5), which is roughly distributed in the cluster of the FZ760 breccia data. Furthermore, the CM-bearing gouge of the Jiulong trench was not found in the WFSD-3 borehole cores [30]. Our RSCM implies that the rock series of the Jiulong trench might be correlated with the Yingxiu–Beichuan fault instead of the Anxian–Guanxian fault.

In summary, we examined samples from the trench at Jiulong, which was deformed during the 2008 M_W-7.9 Wenchuan earthquake, and the following observations and conclusions can be made.

1. The mineralogical and geochemical analyses show the presence of dickite as well as a relative chemical enrichment of Ti and a relative depletion of K within the yellowish HIZ, possibly suggesting the presence of high-temperature fluid–rock interactions.

2. The spectrometric spectra exhibit the absence of CM within the HIZ, possibly resulting from CM pyrolysis.

3. The occurrence of the yellowish gouge suggests its formation is limited to a narrow and localized process. Both the sharp boundary within the very recent coseismic rupture zone of the 2008 M_W-7.9 Wenchuan earthquake and the presence of dickite, which is kinetically unstable on the surface, strongly imply that the yellow/altered gouge likely formed from a recent coseismic event as the consequence of hydrothermal fluid penetration.

4. The RSCM of the CM-bearing gouge falls within the recognized range of graphitization in the FZ760 of WFSD-1, implying a correlation with the Yingxiu–Beichuan fault. We further surmise that the CM characteristics varied according to a driving reaction, e.g., transient hydrothermal heating versus long-term geological metamorphism and sedimentation.

Conflicts of Interest: The authors declare no conflict of interest.

References

1. Sibson, R.H.; Scott, J. Stress-fault controls on the containment and release of overpressured fluids: Examples from gold-quartz vein systems in Juneau, Alaska; Victoria, Australia and Otago, New Zealand. *Ore Geol. Rev.* **1998**, *13*, 293–306. [CrossRef]
2. Di Luccio, F.; Ventura, G.; Di Giovambattista, R.; Piscini, A.; Cinti, F.R. Normal faults and thrusts reactivated by deep fluids: The 6 April 2009 Mw 6.3 L'Aquila earthquake, central Italy. *J. Geophys. Res.* **2010**, *115*. [CrossRef]
3. Lachenbruch, A.H.; Sass, J.H. Heat flow and energetics of the San Andreas fault zone. *J. Geophys. Res.* **1980**, *85*, 6185–6222. [CrossRef]
4. Chester, F.M.; Logan, J.M. Composite planar fabric of gouge from the Punchbowl fault, California. *J. Struct. Geol.* **1986**, *9*, 621–634. [CrossRef]
5. Chester, F.M.; Evans, J.P.; Biegel, R.L. Internal structure and weakening mechanisms of the San Andreas fault. *J. Geophys. Res.* **1993**, *98*, 771–786. [CrossRef]
6. Hickman, S.; Sibson, R.; Bruhn, R. Introduction to special section: Mechanical involvement of fluids in faulting. *J. Geophys. Res.* **1995**, *100*, 12831–12840. [CrossRef]
7. Sibson, R.H. Earthquake rupturing in fluid-overpressured crust: How common? *Pure Appl. Geophys.* **2014**, *171*, 2867–2885. [CrossRef]
8. Engelder, T. The role of pore water circulation during the deformation of foreland folds and thrust belts. *J. Geophys. Res.* **1984**, *89*, 4319–4325. [CrossRef]
9. Kerrich, R. Fluid infiltration into fault zones: Chemical, isotopic and mechanical effects. *Pure Appl. Geophys.* **1986**, *124*, 225–268. [CrossRef]
10. Reynolds, S.J.; Lister, G. Structural aspects of fluid-rock interactions in detachment zones. *Geology* **1987**, *15*, 362–365. [CrossRef]
11. Mccaig, A.M. Deep fluid circulation in fault zones. *Geology* **1988**, *16*, 865–960. [CrossRef]
12. Forster, C.B.; Evans, J.P. Hydrogeology of thrust faults and crystalline thrust sheets: Results of combined field and modeling studies. *Geophys. Res. Lett.* **1991**, *18*, 979–982. [CrossRef]

13. Menzies, C.D.; Teagle, D.A.H.; Niedermann, S.; Cox, S.C.; Craw, D.; Zimmer, M.; Cooper, M.J.; Erzinger, J. The fluid budget of a continental plate boundary fault: Quantification from the Alpine Fault, New Zealand. *Earth Planet. Sci. Lett.* **2016**, *445*, 125–135. [CrossRef]

14. Smeraglia, L.; Berra, F.; Billi, A.; Boschi, C.; Carminati, E.; Doglioni, C. Origin and role of fluids involved in the seismic cycle of extensional faults in carbonate rocks. *Earth Planet. Sci. Lett.* **2016**, *450*, 292–305. [CrossRef]

15. Sibson, R.H. Earthquake rupturing as a mineralizing agent in hydrothermal systems. *Geology* **1987**, *15*, 701–704. [CrossRef]

16. Brantley, S.L.; Evans, B.; Hickman, S.H.; Crerar, D.A. Healing of microcracks in quartz: Implications for fluid flow. *Geology* **1990**, *18*, 136–139. [CrossRef]

17. Glazner, A.F.; Bartley, J.M. Volume loss, fluid flow and state of strain in extensional mylonits from the central Mojave Desert, California. *J. Struct. Geol.* **1991**, *13*, 587–594. [CrossRef]

18. Chen, W.M.D.; Tanaka, H.; Huang, H.J.; Lu, C.B.; Lee, C.Y.; Wang, C.Y. Fluid infiltration associated with seismic faulting: Examining chemical and mineralogical compositions of fault rocks from the active Chelungpu fault. *Tectonophysic* **2007**, *443*, 243–254. [CrossRef]

19. Fu, B.H.; Wang, P.; Kong, P.; Shi, P.L. Preliminary study of coseismic fault gouge occurred in the slip zone of Wenchuan Ms 8.0 earth-quake and its tectonic implications. *Acta Petrol. Sin.* **2008**, *24*, 2237–2243. (In Chinese)

20. Fu, B.H.; Shi, P.L.; Guo, H.D.; Satoshi, O.; Yoshiki, N.; Sarah, W. Surface deformation related to the 2008 Wenchuan earthquake, and mountain building of the Longmenshan, eastern Tibetan Plateau. *J. Asian Earth Sci.* **2011**, *40*, 805–824. [CrossRef]

21. Li, H.B.; Fu, X.F.; Jerone, V.D.W.; Si, J.L.; Wang, Z.X.; Hou, L.W.; Qiu, Z.L.; Li, N.; Wu, F.Y.; Tapponnier, P. Co-seismic surface rupture and dextral-slip oblique thrusting of the Ms 8.0 Wenchuan earthquake. *Acta Geol. Sin.* **2008**, *82*, 1623–1643. (In Chinese)

22. Liu, J.; Zhang, Z.H.; Wen, L.; Sun, J.; Xing, X.C.; Hu, G.Y.; Xu, Q.; Tapponnire, P.; Zeng, L.S.; Ding, L.; et al. The Ms 8.0 Wenchuan earthquake co-seismic rupture and its tectonic implications: An out of sequence thrusting event with slip partitioned on multiple faults. *Acta Geol. Sin.* **2008**, *82*, 1707–1722. (In Chinese)

23. Xu, X.W.; Wen, X.Z.; Yu, G.H.; Chen, G.H.; Klinger, Y.; Hubbard, J.; Shaw, J. Coseismic reverse- and oblique-slip surface faulting generated by the 2008 Mw 7.9 Wenchuan earthquake, China. *Geology* **2009**, *37*, 515–518. [CrossRef]

24. Kuo, L.W.; Li, H.B.; Smith, S.A.F.; Toro, G.D.T.; Suppe, J.; Song, S.R.; Nielsen, S.; Sheu, H.S.; Si, J.L. Gouge graphitization and dynamic fault weakening during the 2008 Mw 7.9 Wenchuan earthquake. *Geology* **2014**, *42*, 47–50. [CrossRef]

25. Kuo, L.W.; Felice, F.D.; Spagnuolo, E.; Toro, G.D.T.; Song, S.R.; Aretusini, S.; Li, H.B.; Suppe, J.; Si, J.L.; Wen, C.Y. Fault gouge graphitization as evidence of past seismic slip. *Geology* **2017**, *45*, 979–982. [CrossRef]

26. Liu, D.L.; Li, H.B.; Lee, T.Q.; Chou, Y.M.; Song, S.R.; Sun, Z.M.; Chevalier, M.L.; Si, J.L. Primary rock magnetism for the Wenchuan earthquake fault zone at Jiulong outcrop, Sichuan Province, China. *Tectonophysics* **2014**, *619–620*, 58–69. [CrossRef]

27. Lin, A.M.; Maruyama, T.; Kobayashi, K. Tectonic implications of damage zone-related fault-fracture networks revealed in drill core through the Nojima fault, Japan. *Tectonophysics* **2007**, *443*, 16–173. [CrossRef]

28. Sibson, R.H. Fault rocks and fault mechanisms. *J. Geol. Soc.* **1977**, *133*, 191–213. [CrossRef]

29. Caine, J.S. Fault zone architecture and permeability structure. *Geology* **1996**, *24*, 1025–1028. [CrossRef]

30. Li, H.B.; Wang, H.; Yang, G.; Xu, Z.Q.; Li, T.F.; Si, J.L.; Sun, Z.M.; Huang, Y.; Chevalier, M.L.; Zhang, W.J.; et al. Lithological and structural characterization of the Longmenshan fault belt from the 3rd hole of the Wenchuan Earthquake Fault Scienti c Drilling project (WFSD-3). *Int. J. Earth Sci.* **2015**, *105*, 2253–2272. [CrossRef]

31. Kuo, L.W.; Song, S.R.; Huang, L.; Yeh, E.C.; Chen, H.F. Temperature estimates of coseismic heating in clay-rich fault gouges, the Chelungpu fault zones, Taiwan. *Tectonophysics* **2011**, *502*, 315–327. [CrossRef]

32. Wopenka, B.; Pasteris, J.D. Structural characterization of kerogens to granulite-facies graphite: Applicability of Raman micro-probe spectroscopy. *Am. Mineral.* **1993**, *78*, 533–557.

33. Beyssac, O.; Goffe, B.; Chopin, C.; Rouzaud, J.N. Raman spectra of carbonaceous material in metasediments: A new geothermometer. *J. Metamorph. Geol.* **2002**, *20*, 859–871. [CrossRef]

34. Ssdezky, A.; Muckenhuber, H.; Grothe, H.; Niessner, R.; Pöschl, U. Raman microspectroscopy of soot and related carbonaceous materials-spectral analysis and structural information. *Carbon* **2005**, *43*, 1731–1742. [CrossRef]

35. Furuichi, H.; Ujiie, K.; Kouketsu, Y.; Saito, T.; Tsutsumi, A.; Wallis, S. Vitrinite reflectance and Raman spectra of carbonaceous material as indicators of frictional heating on faults: Constraints from friction experiments. *Earth Planet. Sci. Lett.* **2015**, *424*, 191–200. [CrossRef]

36. Liu, Z.; Colin, C.; Huang, W.; Le, K.P.; Tong, S.; Chen, Z.; Trentesaux, A. Climatic and tectonic controls on weathering in South China and the Indochina Peninsula: Clay mineralogical and geochemical investigations from the Pearl, Red, and Mekong drainage basins. *Geochem. Geophys. Geosyst.* **2007**, *8*, Q05005. [CrossRef]

37. Kuo, L.W.; Song, S.R.; Yeh, E.C.; Chen, H.F. Clay mineral anomalies in the fault zone of the Chelungpu Fault, Taiwan, and their implications. *Geophys. Res. Lett.* **2009**, *36*, L18306. [CrossRef]

38. Kuo, L.W.; Song, S.R.; Yeh, E.C.; Chen, H.F.; Si, J.L. Clay mineralogy and geochemistry investigations in the host rocks of the Chelungpu fault, Taiwan: Implication for faulting mechanism. *J. Asian Earth Sci.* **2012**, *59*, 208–218. [CrossRef]

39. Lunsdorf, N.K.; Dunkl, I.; Schmidt, B.C.; Rantitsch, G.; van Eynatten, H. Towards a higher comparibility of geothermetric data obtained by ramen spectroscopy of carbonaceous material. Part 1: Evaluation of biasing factors. *Geostand. Geoanal. Res.* **2014**, *38*, 73–94. [CrossRef]

40. Lunsdorf, N.K.; Dunkl, I.; Schmidt, B.C.; Rantitsch, G.; van Eynatten, H. Towards a higher comparibility of geothermetric data obtained by ramen spectroscopy of carbonaceous material. Part 2: A revised geothermometer. *Geostand. Geoanal. Res.* **2017**, *41*, 593–612. [CrossRef]

41. Kuo, L.W.; Huang, J.R.; Fang, J.N.; Si, J.L.; Song, S.R.; Li, H.B.; Yeh, E.C. Carbonaceous materials in the fault zone of the Longmenshan Fault belt: 2. From drilling and implications for fault maturity. *Minerals* **2018**, *8*, 393. [CrossRef]

42. Evans, J.P.; Chester, F.M. Fluid–rock interaction in faults of the San Andreas system: Inferences from San Gabriel fault rock geochemistry and microstructures. *J. Geophys. Res.* **1995**, *100*, 13007–13020. [CrossRef]

43. Goddard, J.V.; Evans, J.P. Chemical changes and fluid–rock interaction in faults of crystalline thrust sheets, northwestern Wyoming, U.S.A. *J. Struct. Geol.* **1995**, *17*, 533–547. [CrossRef]

44. Tanaka, H.; Fujimoto, K.; Ohtani, T.; Ito, H. Structural and chemical characterization of shear zones in the freshly activated Nojima fault, Awaji Island, southwest Japan. *J. Geophys. Res.* **2001**, *106*, 8789–8810. [CrossRef]

45. Grim, R.E. *Clay Mineralogy*, 2nd ed.; McGraw-Hill Company: New York, NY, USA, 1969; 596p.

46. Keller, W.D. Environmental aspects of clay minerals. *J. Sediment. Petrol.* **1970**, *4*, 788–813.

47. Lin, S.B.; Wang, Y.R. Mineralogy and tectonic implication of the dickites from Hengchun Peninsula, southern Taiwan. *Acta Geol. Taiwan* **1989**, *27*, 19–32.

48. Barker, C.E.; Goldstein, R.H. Fluid-inclusion technique for determining maximum temperature in calcite and its comparison to the vitrinite reflectance geothermometer. *Geology* **1990**, *18*, 1003–1006. [CrossRef]

49. Beyssac, Q.; Goffeé, B.; Petitet, J.P.; Froigneux, E.; Moreau, M.; Rouzaud, J.N. On the characterization of disordered and heterogeneous carbonaceousmaterials by Raman spectroscopy. *Spectrochim. Acta Part A Mol. Biomol. Spectrosc.* **2003**, *59*, 2267–2276. [CrossRef]

50. Kouketsu, Y.; Shimizu, I.; Wang, Y.; Ma, S.L.; Shimamoto, T. Raman spectra of carbonaceous materials in a fault zone in the Longmenshan thrust belt, China; comparisons with those of sedimentary and metamorphic rocks. *Tectonophysics* **2017**, *699*, 129–145. [CrossRef]

51. Ma, K.F.; Song, T.R.A.; Lee, S.J.; Wu, H.I. Spatial slip distribution of the September 20, 1999, Chi-Chi, Taiwan, Earthquake (Mw 7.6)—inverted from teleseismic data. *Geophys. Res. Lett.* **2000**, *27*, 3417–3420. [CrossRef]

52. Chen, Y.G.; Chen, W.S.; Lee, J.C.; Lee, Y.H.; Lee, C.T.; Chang, H.C.; Lo, C.H. Surface rupture of the 1999 Chi-Chi earthquake yields insights on the active tectonics of central Taiwan. *Bull. Seismol. Soc. Am.* **2001**, *91*, 977–985. [CrossRef]

53. Ishikawa, T.; Tanimizu, M.; Nagaishi, K.; Matsuoka, J.; Tadai, O.; Sakaguchi, M.; Kikuta, H. Coseismic fluid–rock interactions at high temperatures in the Chelungpu fault. *Nat. Geosci.* **2008**, *1*, 679. [CrossRef]

54. Mizoguchi, K.; Takahashi, M.; Tanikawa, W.; Masuda, K.; Song, S.R.; Soh, W. Frictional strength of fault gouge in Taiwan Chelungpu fault obtained from TCDP Hole, B. *Tectonophysics* **2008**, *460*, 198–205. [CrossRef]

55. Hirono, T.; Maekawa, Y.; Yabuta, H. Investigation of the records of earthquake slip in carbonaceous materials from the Taiwan Chelungpu fault by means of infrared and Raman spectroscopies. *Geochem. Geophys. Geosyst.* **2015**, *16*, 1233–1253. [CrossRef]

56. Viesca, R.C.; Garagash, D.I. Ubiquitous weakening of faults due to thermal pressurization. *Nat. Geosci.* **2015**, *8*, 875–879. [CrossRef]
57. Chen, J.; Yang, X.; Duan, Q.; Shimamoto, T.; Spiers, C.J. Importance of thermochemical pressurization in the dynamic weakening of the Longmenshan fault during the 2008 Wenchuan earthquake: Inferences from experiments and modeling. *J. Geophys. Res.* **2013**, *118*, 4145–4169. [CrossRef]